

Coupling and decoupling of spin crossover and ferroelastic distortion: Unsymmetric hysteresis loop, phase diagram, and sequence of phases

Eric Collet^{*} and Giovanni Azzolina[†]*Univ Rennes, CNRS, IPR (Institut de Physique de Rennes) - UMR 6251, F-35000 Rennes, France*
 (Received 14 January 2021; revised 11 March 2021; accepted 16 March 2021; published 1 April 2021)

Spin-transition materials can exhibit thermal hysteresis due to cooperative elastic interactions in between active molecular sites. It results from the coupling of the nonsymmetry-breaking high spin fraction order parameter to the lattice volume strain. However, a symmetry-breaking order parameter responsible for crystallographic phase transition, like a ferroelastic distortion, can also couple to the volume strain. Here, we use the Landau theory to study the elastic coupling between a spin-crossover instability and a discontinuous ferroelastic distortion and the different phase transition lines. Below the triple point, the first-order line involves simultaneous ferroelastic distortion and spin transition. Above, the purely first-order ferroelastic distortion and the spin crossover occur sequentially. Our model, related to the coupling and decoupling of the ferroelastic phase transition and spin crossover, explains exotic behaviors reported experimentally in the literature for diverse spin-crossover systems, plastic crystals, or Prussian blue analogues. The unsymmetric hysteresis loops and the stepwise evolution of the spin conversion or volume strain under pressure result from different sequences of phase transitions. The model shows that the ferroelastic phase transition is the driving force of the cooperative spin transition hysteresis in this case.

DOI: [10.1103/PhysRevMaterials.5.044401](https://doi.org/10.1103/PhysRevMaterials.5.044401)

I. INTRODUCTION

Spin crossover, and more precisely spin transition, is currently a hot topic, aiming at playing on molecular bistability to produce compounds with wide hysteresis loops between low-spin (LS) and high-spin (HS) phases [1–4]. Tuning the domain of bistability over a broad temperature range, especially around room temperature, or generating and controlling multistep and hysteretic spin transitions represent important targets. Spin-crossover materials also exhibit multifunctionalities [5,6], as the spin transition can be triggered by pressure [7–9], inclusion of guests [10,11], or by light excitation [12,13] down to the femtosecond timescale [14–17]. It was recently shown that spin-crossover materials represent a promising route for biomimetic soft actuators [18]. In many cases, the spin transition between HS and LS state is nonsymmetry breaking [3,19,20]. From the experimental point of view, a symmetry change, like a ferroelastic structural phase transition, concomitant to a spin transition was pointed to as a factor influencing the hysteretic behavior in terms of broadening and shape [21–29]. Ferroelasticity is a phenomenon in which, due to a symmetry-breaking phase transition between different crystalline systems, a material exhibits a spontaneous strain in the low-symmetry (ls) phase [30]. However, in several samples, the identification of the symmetry change is not possible, as crystals crumble during the phase transition due to large structural reorganizations and volume strain, i.e., the volume contraction accompanying the HS-to-LS conversion

[31]. Seredyuk *et al.* [32] underlined the role of structural reorganizations and symmetry change in the broadening of the hysteresis with the $[\text{Fe}(\text{nBu-im})_3(\text{tren})](\text{PF}_6)_2$ complex. The 14 K wide thermal hysteresis, when the lattice does not rearrange, increases to 41 K when a large conformational change of butyl substituent PF_6^- anions occurs. Halcrow [33] and Reeves *et al.* [34] and many others also underlined that structural rearrangements during the transition and strong intermolecular interactions are two factors increasing the thermal hysteresis width [35].

The prototype $[\text{Fe}(\text{ptz})_6](\text{BF}_4)_2$ system was intensively investigated in the literature [22,36–42]. It exhibits a thermal spin-transition hysteresis, coupled to a ferroelastic structural phase transition from the HS ($R\bar{3}$) phase, toward the LS $P\bar{1}$ phase. As shown in the review paper by Gütllich *et al.* [36], the hysteresis loop is unsymmetric [Fig. 1(a)]. Lemée-Cailleau *et al.* [43] evidenced that the ferroelastic transition and spin crossover occur sequentially under pressure. A similar situation is found in plastic organic crystals, like the nitroxyl radical 1-methyl-2-azaadamantane N-oxyl (Me-AZADO), which exhibits magnetic bistability arising from a radical-dimer interconversion. Dragulescu-Andrasi *et al.* [44] have shown that (Me-AZADO) exhibits magnetic bistability [Fig. 1(b)] from a paramagnetic ($S = \frac{1}{2}$) hexagonal ($P6_3/m$) phase with disordered radicals to an ordered and diamagnetic ($S = 0$) orthorhombic ($Pbca$) phase. The $[\text{Co}^{\text{II}}(\text{dpzca})_2]$ systems investigated by Cowan *et al.* [45] and Miller *et al.* [46] [Fig. 1(c)] also exhibit a phase transition from a HS tetragonal ($I4_1/a$) phase to a LS monoclinic ($P2_1/c$) phase. These three systems represent a diversity of materials for which the change of spin state couples to a ferroelastic transition from the HS high-symmetry (HSHs) phase to the LSLs phase.

*eric.collet@univ-rennes1.fr

†giovanni.azzolina@univ-rennes1.fr

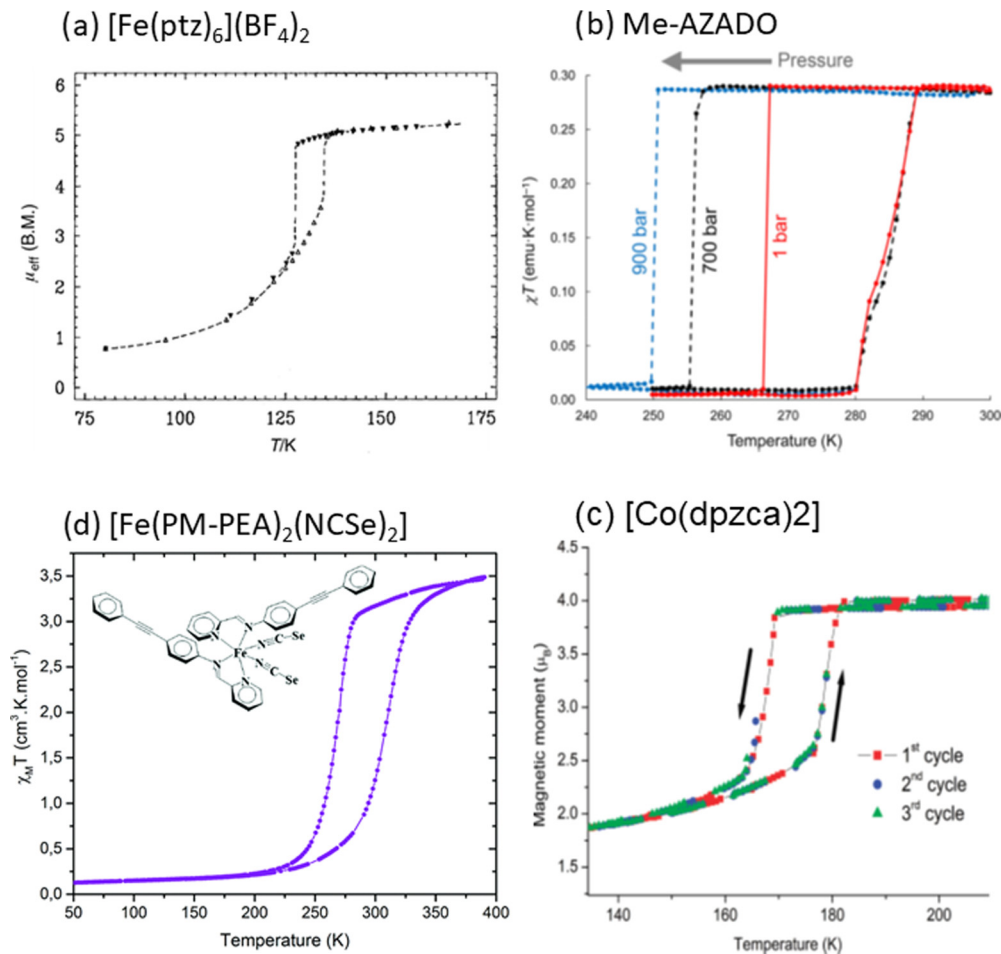


FIG. 1. The unsymmetric spin-transition hysteresis loop of a few systems for which the spin transition is coupled to a ferroelastic symmetry-breaking. (a) $[\text{Fe}(\text{ptz})_6](\text{BF}_4)_2$, reprinted with permission from Ref. [36]. (b) Me-AZADO, reprinted with permission from Ref. [44]. (c) $[\text{Co}(\text{dpzca})_2]$, reprinted with permission from Ref. [45]. (d) $\text{Fe}(\text{PM-pea})_2(\text{NCSe})_2$, reproduced with permission from Ref. [50].

There are many other types of systems for which this is the case, including MnFe Prussian blue analogues undergoing a cubic-tetragonal ferroelastic distortion related to Jahn-Teller distortion coupled to charge transfer [26] or Mn materials undergoing spin crossover coupled to monoclinic-triclinic ferroelastic distortion that is responsible for giant magneto-electric coupling [47,48]. A different situation is reported for the $\text{Fe}(\text{PM-pea})_2(\text{NCS})_2$ and $\text{Fe}(\text{PM-pea})_2(\text{NCSe})_2$ systems investigated by Guionneau *et al.* [49], Tailleux *et al.* [50], and Létard *et al.* [51]. These compounds exhibit very unusual spin transitions as the low-temperature LS phase is the hs phase (LS_{hs}, orthorhombic), and the HS phase is the ls one (HS_{ls}, monoclinic). Here again, the thermal spin transition hysteresis loops are wide and unsymmetric [Fig. 1(d)] with complex behavior under pressure.

From the theoretical point of view, the thermodynamical aspects of spin-crossover phenomena have been largely investigated by various methods, considering crystal field theory, entropy, formation of domains, and elastic interactions, to name a few [52–61]. The Slichter-Drickamer model is also often used to describe cooperative spin transition [62]. Other theoretical works have focused on the elastic interaction due to the volume change associated with the change of spin state only [52,63–65]. All these models often provide quite

symmetric thermal spin crossover or hysteresis. However, the symmetry-breaking aspect that may accompany spin transitions or spin crossovers is generally not considered, except for describing spin-state ordering phenomena, i.e., the formation of spin-state concentration waves in stepwise spin-state conversion [63,66–68]. A phenomenological Ising-like model [69] was also introduced to describe the effect of the concurrent ordering of solvent molecules and the spin conversion but did not consider the elastic coupling energy.

In the case of a symmetry-breaking ferroelastic phase transition, i.e., when the crystal system changes (from cubic to tetragonal, rhombohedral to triclinic, orthorhombic to monoclinic, etc.), a spontaneous strain appears in the ls phase, and the symmetry change couples to a volume strain [30,70]. Since the volume strain is also the driving force of cooperative spin transition, both symmetry-breaking ferroelastic phase transition and spin conversion may couple through the volume strain, which may be responsible for unusual response to external stimuli. In this paper, we focus our attention on the elastic coupling between nonsymmetry-breaking spin crossover and symmetry-breaking structural distortions. We show that this coupling enhances the regime of bistability in the phase diagram, gives rise to unsymmetric hysteresis loops, and generates different phases. The spin crossover and the

ferroelastic distortion may therefore occur simultaneously or sequentially.

II. SPIN TRANSITION COUPLED TO SYMMETRY BREAKING

A. Order parameters and model

The spin transition in materials is represented by an Ising variable q_i , describing the spin state of the i th molecular site: $q_i = 1$ (HS) or $q_i = -1$ (LS), as often used in different models [52,53,59,66,71,72]. The spin-state conversion is then monitored through the average q or the average fraction γ of HS molecules:

$$q = \frac{N_{\text{HS}} - N_{\text{LS}}}{N_{\text{HS}} + N_{\text{LS}}} \quad \text{or} \quad \gamma = \frac{N_{\text{HS}}}{N_{\text{HS}} + N_{\text{LS}}} \quad \text{with} \quad \gamma = \frac{q + 1}{2}, \quad (1)$$

where N_{HS} and N_{LS} denote the number of sites in HS or LS states. In the fully HS state, the average HS fraction $\gamma = 1$ ($q = 1$), while in the fully LS state $\gamma = 0$ ($q = -1$). A spin crossover is a gradual evolution of the HS fraction from $\gamma = 0$ to 1, while the discontinuous evolution, eventually associated with a thermal hysteresis, corresponds to a spin transition [20]. In addition to the change of spin state, spin-transition materials can exhibit symmetry change of various natures [73]. Here, we are interested in systems exhibiting a ferroelastic phase transition coupled to the spin crossover. For example, $[\text{Co}(\text{dpzca})_2]$ exhibits an abrupt and complete spin transition coupled to a ferroelastic transition from tetragonal ($I4_1/a$) to monoclinic ($P2_1/c$) phase [45,46]. There is a group-subgroup relationship between the high- and low-temperature phases, and the Landau theory applies. It is necessary to use a symmetry-breaking order parameter η for monitoring the ferroelastic transition and characterizing the deviation from the tetragonal symmetry in the low-temperature phase. In this case, η is scalar, as it belongs to the one-dimensional B_g representation of the $4/m$ point group [74,75]. In the hs phase $\eta = 0$, and in the ls phase, two domains form ($\pm\eta$), equivalent by symmetry. The thermodynamical potential Φ must therefore fulfill the relationship $\Phi(-\eta) = \Phi(\eta)$ and consequently includes only even orders in η .

In these volume-changing phase transitions, where molecular-based deformations propagate at the macroscopic scale within the crystal, it is essential to consider elastic energy terms. On the one hand, the spontaneous strain $e \propto \eta$, associated with the tetragonal-monoclinic ferroelastic distortions, is responsible for a volume strain $v_\eta \propto \eta^2$ [70]. On the other hand, in the case of the nonsymmetry-breaking spin conversion, the associated change in the bonding nature of the lattice is responsible for a volume strain $v_q \propto (\frac{1-q}{2})$ [26]. The symmetry-breaking ferroelastic and the nonsymmetry-breaking spin-transition volume strains contribute to the total volume strain, which is the relative volume change compared with the HShs phase: $v_s = \frac{v(T) - v_{\text{HShs}}}{v_{\text{HShs}}} = v_\eta + v_q$.

The Landau theory allows describing the evolution of the thermodynamical potential around the phase transition temperature through its expansion in power series of the order parameters $\Phi(\eta, q)$. We have recently discussed the case where a nonsymmetry-breaking order parameter q , here, monitoring spin conversion, and a symmetry-breaking order

parameter η , describing here ferroelastic distortion, may couple [26]. Based on this previous paper, the potential reduces here to

$$\Phi = \frac{1}{2}a\eta^2 + \frac{1}{4}b\eta^4 + \frac{1}{6}c\eta^6 + Aq + \frac{1}{2}Bq^2 + \frac{1}{4}Cq^4 + \lambda_\eta v_s \eta^2 + \lambda_q v_s \left(\frac{1-q}{2}\right) + \frac{1}{2}C_s^0 v_s^2. \quad (2)$$

The η^2, η^4, η^6 terms describe the symmetry breaking, with $a = a_0(T - T_{\text{SB}})$ at constant pressure and $c > 0$ for stability. Here, we use $b < 0$, which describes a first-order ferroelastic transition [30]. The coefficient a changes sign with temperature T at T_{SB} . The hs phase ($\eta = 0$) is stable down to T_{SB} , the symmetry-breaking temperature. The ls phase ($\eta \neq 0$) is stable up to $T_1 = \frac{b^2}{8ac} + T_{\text{SB}}$. The symmetry-breaking curve $\eta^2(T)$ exhibits a thermal hysteresis and changes discontinuously at T_{SB} and T_1 . The q, q^2, q^4 terms describe the spin conversion with $A = a_0(T_{\text{SC}} - T)$ and $C > 0$ for stability. Here, we use $B > 0$, which corresponds to a spin crossover. It describes a gradual change from $q > 0$ above T_{SC} to $q < 0$ below, i.e., from HS ($\gamma = 1$) at high temperature to LS ($\gamma = 0$) at low temperature. For limiting the number of parameters, we will consider hereafter b and B constant. Here, $\frac{1}{2}C_s^0 v_s^2$ is the elastic energy related to elastic constant C_s^0 and the total volume strain v_s . Also, $\lambda_\eta v_s \eta^2$ is the elastic coupling to v_s of the ferroelastic distortion and is zero in the hs phase. Further, $\lambda_q v_s (\frac{1-q}{2})$ is the elastic coupling to v_s of the spin transition and is zero in fully HS phase. The equilibrium volume strain minimizing the potential is

$$v_s = -\frac{[\lambda_q (\frac{1-q}{2}) + \lambda_\eta \eta^2]}{C_s^0} = -\left[\alpha \left(\frac{1-q}{2}\right) + \beta \eta^2\right] = v_q + v_\eta. \quad (3)$$

Substituting v_s in Eq. (2) renormalizes some coefficients of the Landau expansion:

$$\Phi = \frac{1}{2} \left(a - \frac{\lambda_\eta \lambda_q}{C_s^0} \right) \eta^2 + \frac{1}{4} b \eta^4 + \frac{1}{6} \left(c - \frac{\lambda_\eta^2}{2C_s^0} \right) \eta^6 + \left(A + \frac{\lambda_q^2}{4C_s^0} \right) q + \frac{1}{2} \left(B - \frac{\lambda_q^2}{8C_s^0} \right) q^2 + \frac{1}{4} C q^4 + \left(\frac{\lambda_\eta \lambda_q}{2C_s^0} \right) q \eta^2. \quad (4)$$

The expression highlights that the elastic couplings of q and η to the volume strain lead to an effective linear-quadratic coupling between the order parameters. This elastic coupling also decreases the q^2 coefficient, which makes the spin crossover more cooperative. By renormalizing the coefficients, the expansion of the thermodynamical potential reaches a most simple form:

$$\Phi = \frac{1}{2}a\eta^2 + \frac{1}{4}b\eta^4 + \frac{1}{6}c\eta^6 + Aq + \frac{1}{2}Bq^2 + \frac{1}{4}Cq^4 + Dq\eta^2. \quad (5)$$

The global potential in Eq. (5), with 2-4-6 order terms in η , corresponds to four phases characterized by their spin state (HS for $q > 0$ and LS for $q < 0$) and symmetry (hs for $\eta = 0$ and ls for $\eta \neq 0$): HShs, HSl, LShs, and LSl. Their relative stability depends on the dimensionless temperature T ,

on the temperature difference between the symmetry-breaking and spin-crossover temperatures ($T_{SB} - T_{SC}$), and on the coupling strength D . Here, D is positive for stabilizing the LSIs phase ($q < 0$, $\eta \neq 0$). The pressure effect requires considering the linear dependence of the coefficients a and A with temperature and pressure: $a = a_0(T - T_{SB}) + a_1(P - P_{SB})$ and $A = a_0(T_{SC} - T) + A_1(P_{SC} - P)$. For simplicity, we use the same coefficient a_0 , which is analogous to crossing the phase transition line of the (P, T) phase diagram, not at constant pressure but in an oblique way. Then the difference in the symmetry-breaking and spin-crossover temperature instabilities $T_{SB} - T_{SC} = -\frac{A+a}{a_0} + \frac{A_1}{a_0}P_{SC} - \frac{a_1}{a_0}P_{SB} + \frac{a_1-A_1}{a_0}P$ changes linearly with pressure. Therefore, in the limit of our approximations, $T_{SB} - T_{SC}$ is analogous to pressure, and for avoiding over parametrization, we represent the phase diagram in the $T - T_{SC}$, $T_{SB} - T_{SC}$ space. The equilibrium values of the OP characterize the stability region of the different phases, found by minimizing $\Phi(q, \eta)$:

$$\begin{aligned} \frac{d\Phi}{d\eta} &= 0, & \frac{d\Phi}{dq} &= 0, \\ \frac{d\Phi^2}{d\eta^2} &> 0, & \frac{d\Phi^2}{dq^2} &> 0, & \text{and} & \frac{d\Phi^2}{dq d\eta} > 0. \end{aligned} \quad (6)$$

B. Results

Figure 2(a) shows the phase diagram obtained with the 2-4-6 potential in Eq. (5) and calculated with $b = -6$, $c = 12$, $B = 2$, $C = 12$, and $D = 2$. We are interested in the general qualitative features of the behaviors. Tuning the parameters of the potentials or adding high-order terms allows a qualitative comparison with experiments, but the parameter space to explore is then very large. The temperature T shown in the vertical axis is arbitrarily scaled through the coefficient a_0 , and we choose T_{SC} as the origin. We focus our attention on the HSs, HSLs, and LSLs phases, but in a symmetric way, the LSHs phase forms for $(T_{SB} - T_{SC}) < 0$, as discussed below. This portion of the phase diagram exhibits a triple point around $T - T_{SC} \approx 1.2$; $T_{SB} - T_{SC} \approx 2.6$, where the HSs, HSLs, and LSLs phases coexist, and the hysteretic domain of bistability is shown by the gray shaded area in the phase diagram.

Figure 3 shows the temperature dependence of the order parameters $\gamma(T)$ (also scaled to q), and $\eta^2(T)$ for different values of $T_{SB} - T_{SC}$. Figure 4(a) shows the thermal evolution just below the triple point for $(T_{SB} - T_{SC}) = 1.5$. Here, $\eta^2(T)$ characterizes the ferroelastic transition and measures the deviation from hs, i.e., the deviation from tetragonal lattice in the LSLs phase in the case of $[\text{Co}(\text{dpzca})_2]$, for example [45]. Below the triple point, $\gamma(T)$ and $\eta^2(T)$ both change discontinuously at the same temperatures on cooling and on warming. The spin-transition curves in Figs. 3 and 4(a) mimic the unsymmetric hysteresis loop shown in Fig. 1(b). This effect is more and more pronounced as $T_{SB} - T_{SC}$ increases, with a discontinuous conversion on cooling and a more gradual conversion on warming. This unsymmetric hysteresis loop is due to the $Dq\eta^2$ coupling, which acts only in the LSLs phase where $\eta \neq 0$. The coefficient a is renormalized to $(a + Dq) = a_0(T - T'_{SB})$, with $T'_{SB} = T_{SB} - Dq$, shifting the symmetry breaking toward lower temperature on cooling from

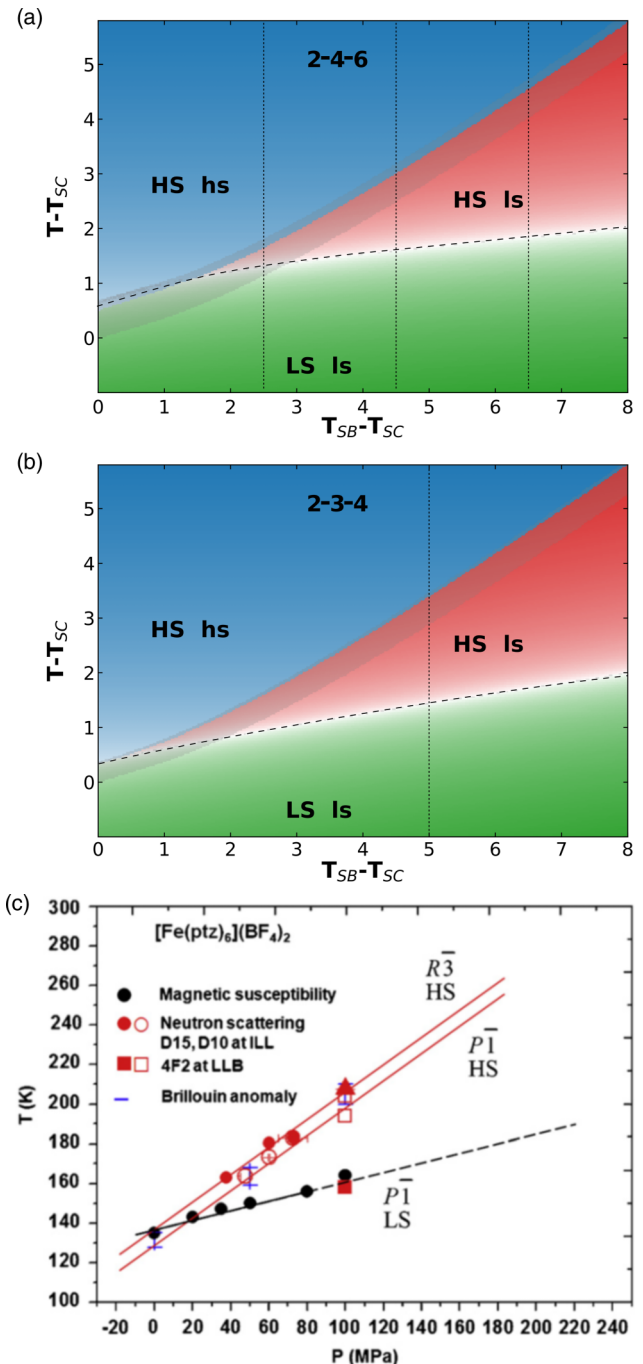


FIG. 2. (a) Phase diagram calculated for the 2-4-6 potential in Eq. (5) with $b = -6$, $c = 12$, $B = 2$, $C = 12$, and $D = 2$. For $T_{SB} - T_{SC} = 0$, the spin conversion and the symmetry breaking occur simultaneously, with a thermal hysteresis between the high-spin, high-symmetry (HSs) and low-spin, low-symmetry (LSs) phases (gray shaded area between hs and ls phases). Above the triple point, a ferroelastic phase transition from HSs to HSLs phases occurs around T_{SB} , followed at lower temperature by a spin crossover (dashed line) from the HSLs to the LSLs phase at $T_{1/2}$. The vertical dotted lines represent the cuts of the phase diagram shown in Fig. 3. (b) Phase diagram calculated for the 2-3-4 potential in Eq. (7), showing analogous behavior. The vertical dotted line corresponds to the cut of the phase diagram shown in Fig. 4(b). (c) Experimental phase diagram reported in Ref. [43] with HSs ($R\bar{3}$), HSLs ($P\bar{1}$), and LSLs ($P\bar{1}$) phases. Reprinted with permission from Ref. [43].

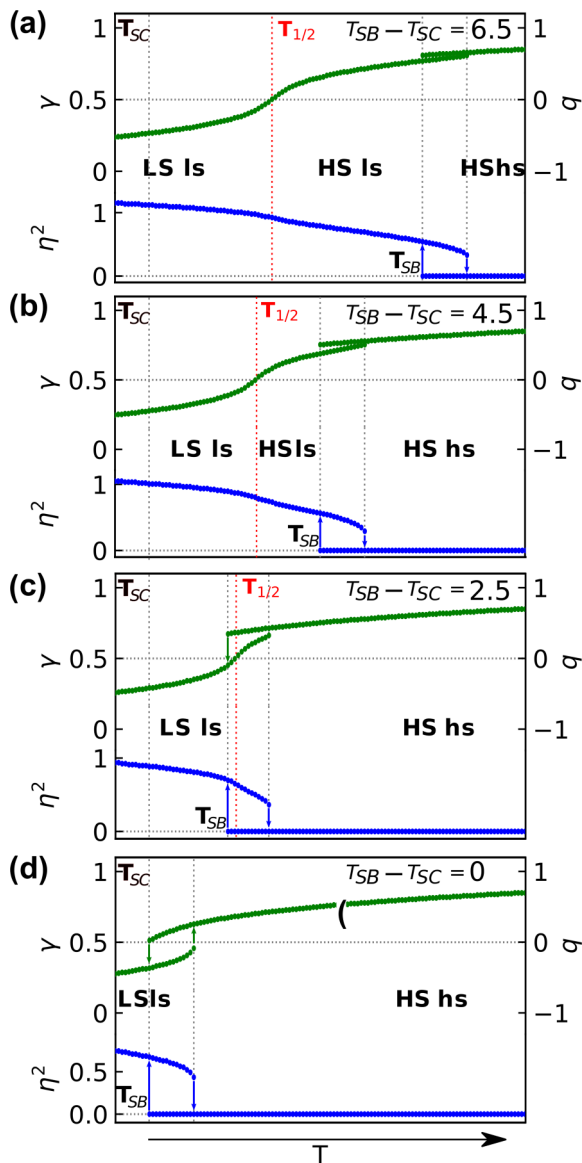


FIG. 3. Spin-transition curves $\gamma(T)$ in green, also scaled in $q(T)$, and symmetry-breaking curves $\eta^2(T)$ in blue, extracted from the phase diagram in Fig. 2(a) for different $T_{SB} - T_{SC}$ [corresponding to the vertical dotted lines in Fig. 2(a)]. Below the triple point, the symmetry breaking and the spin transition occur simultaneously between the high-spin, high-symmetry (HS_{hs}) and low-spin, low-symmetry (LS_{ls}) phases. Above the triple point, on cooling from the HS_{hs} phase, the symmetry breaking occurs first toward the HS_{ls} phases, followed by a spin crossover from the HS_{ls} to the LS_{ls} phase at $T_{1/2}$, where $\gamma = \frac{1}{2}$. As $T_{SB} - T_{SC}$ increases, the ferroelastic phase transition and the spin crossover get more and more separated. $T_{1/2}$ deviates from T_{SC} due to the coupling.

the HS_{hs} phase ($q > 0$) and toward higher temperature on cooling from the LS_{ls} phase ($q < 0$). In a similar way, the coefficient $A = a_0(T_{SC} - T)$ is renormalized to $(A + D\eta^2) = a_0(T'_{SC} - T)$, with $T'_{SC} = T_{SC} + D\eta^2$, which stabilizes the LS state toward higher temperature in the LS_{ls} phase with ($\eta \neq 0$). Therefore, on cooling from the HS_{hs} phase, when symmetry breaking starts ($\eta \neq 0$), the spin transition occurs simultaneously, while on warming, from the LS_{ls} phase,

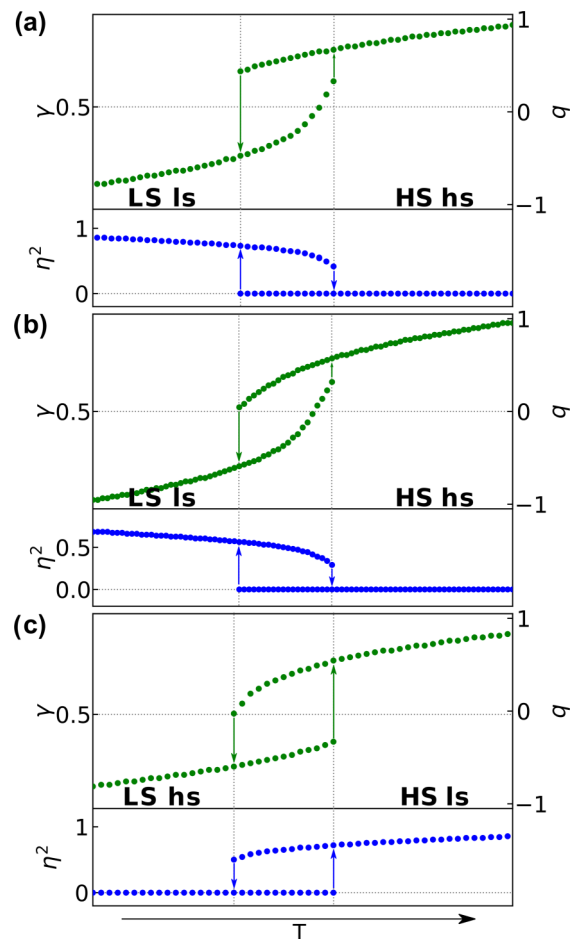


FIG. 4. Unsymmetric spin transition hysteresis loop $\gamma(T)$ and symmetry-breaking curves $\eta^2(T)$ in the vicinity of the triple point. (a) Low-spin, low-symmetry (LS_{ls})–to–high-spin, high-symmetry (HS_{hs}) transition with the 2-4-6 potential in Eq. (5), symmetry adapted to [Co(dpzca)]₂. (b) LS_{ls}-to-HS_{hs} transition with the 2-3-4 potential in Eq. (7), symmetry adapted to [Fe(ptz)₆](BF₄)₂. (c) LS_{hs}-to-HS_{ls} transition with the modified 2-4-6 potential in Eq. (5) symmetry adapted to Fe(PM-pea)₂(NCS)₂ or Fe(PM-pea)₂(NCSe)₂ and using negative values for a and D . The plots have been arbitrarily scaled in temperature scale (a_0) to better compare the hysteresis loop shapes.

where $q < 0$, the coupling stabilizes the LS_{ls} phase toward higher temperature and the spin crossover starts with a gradual conversion, followed by the symmetry change. The coupling shifts therefore the half conversion temperature $T_{1/2}$, where $\gamma = \frac{1}{2}$, toward higher temperature as $T_{SB} - T_{SC}$ increases. This $T_{1/2}$ spin crossover line corresponds to the dashed line in Fig. 2(a).

This result explains therefore that it is the elastic coupling between the spin-crossover (continuous) and the discontinuous ferroelastic phase transition, which is responsible for the appearance of unsymmetric spin-transition hysteresis loops. When pressure increases, or more precisely when $T_{SB} - T_{SC}$ increases, the unsymmetric shape of the spin-transition curve is more pronounced.

An unsymmetric spin-transition hysteresis loop, with a more discontinuous cooling branch and a more gradual warming branch, was also reported for [Fe(ptz)₆](BF₄)₂

[Fig. 1(a)] [36–42]. At atmospheric pressure, the spin conversion is also coupled to a first-order ferroelastic phase transition, and both phenomena occur simultaneously [37]. The space group of the HSHs high-temperature phase is $R\bar{3}$, and on cooling, a first-order phase transition occurs toward the LSIs phase ($P\bar{1}$) [37,76,77]. In this case, the symmetry-breaking order parameter driving the $R\bar{3}$ -to- $P\bar{1}$ ferroelastic transition belongs to the bidimensional E_g representation of the $\bar{3}$ point group, the basis of which is built with two distortion strains [74,75,78,79]. This situation is like the one discussed in the case of the cubic-to-tetragonal ferroelastic transition in RbMnFe [26], and the relevant Landau potential for describing this symmetry breaking includes then 2-3-4 order terms in η :

$$\Phi = \frac{1}{2}a\eta^2 + \frac{1}{3}b\eta^3 + \frac{1}{4}c\eta^4 + Aq + \frac{1}{2}Bq^2 + \frac{1}{4}Cq^4 + Dq\eta^2. \quad (7)$$

Here again, we use $B > 0$, corresponding to a spin crossover, while the symmetry-allowed η^3 term limits the $R\bar{3}$ -to- $P\bar{1}$ ferroelastic transition to first order only. The phase diagram obtained with this potential in Eq. (7) and shown in Fig. 2(b) is qualitatively similar to the one obtained with the potential in Eq. (5) in Fig. 2(a) because both correspond to the coupling between a first-order ferroelastic transition and a spin crossover. Figure 4(b) shows typical spin-transition and symmetry-breaking curves obtained with the potential in Eq. (7) just below the triple point [corresponding to the dotted vertical line in Fig. 2(b)], like the ones obtained with the potential in Eq. (5) in Fig. 4(a) and reproducing the unsymmetric hysteresis loop.

Another interesting point to discuss is the effect of pressure, which shifts differently T_{SB} and T_{SC} . As shown in Figs. 2 and 3 for the potentials in Eqs. (5) and (7), above the triple point, a spin crossover occurs around $T_{1/2}$, with a gradual evolution of $\gamma(T)$, followed by a discontinuous change around T_{SB} , where the symmetry change occurs, due to the coupling. Here, $\eta^2(T)$ changes discontinuously around T_{SB} and exhibits a continuous evolution around T_{SC} . Therefore, above the triple point, the apparent stepwise spin conversion curve $\gamma(T)$ results from a spin crossover at $T_{1/2}$ and a discontinuous change due to the ferroelastic transition.

Interestingly, the neutron diffraction study of $[\text{Fe}(\text{ptz})_6](\text{BF}_4)_2$ performed by Lemée-Cailleau *et al.* [9,43] evidenced that, under pressure, the ferroelastic phase transition is dissociated from the spin crossover in the phase diagram [Fig. 2(c)]. Above the triple point, the transition lines are then characterized by two anomalies of the lattice parameters [Fig. 5(a)], in the form of a discontinuous change at the ferroelastic phase transition, with a thermal hysteresis, and a gradual change at the spin crossover [9]. At 100 MPa, the spin crossover from LSIs ($P\bar{1}$) to HSHs ($P\bar{1}$) occurs around 155 K without symmetry change, while a first-order ferroelastic phase transition occurs around 200 K from HSHs ($P\bar{1}$) to HSHs ($R\bar{3}$). In other words, an intermediate HSHs $P\bar{1}$ phase appears under pressure. The hysteresis phenomenon was fully attributed to the ferroelastic phase transition, as its first-order nature does not depend on pressure. Indeed, in the case of $[\text{Fe}(\text{ptz})_6](\text{BF}_4)_2$, the bidimensional nature of the order parameter restricts symmetry breaking to first order,

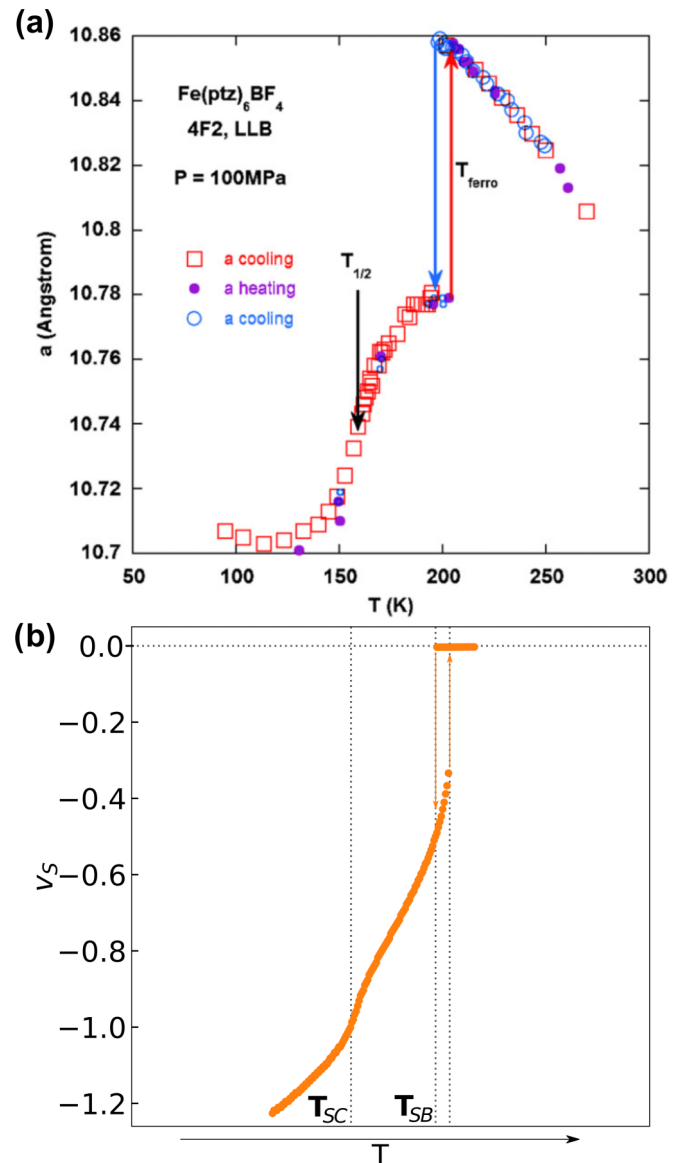


FIG. 5. (a) Evolution of the a cell parameter vs temperature at 100 MPa with a jump at the ferroelastic transition with a hysteresis (at T_{ferro}) and a continuous change at lower temperature associated with the spin crossover (at $T_{1/2}$). Reprinted with permission from Ref. [9]. (b) Evolution of the total volume strain given by Eq. (3), clearly separating the contribution above the triple point of each order parameter to the volume strain. The volume of the high-spin, high-symmetry (HSHs) phase is taken as reference, and we used $\beta = 50\alpha$ to mimic the evolution of the a cell parameter.

as mentioned above. This sequence of HSHs, HSHs, and LSIs phases shown in Fig. 5(a) corresponds then to the top panel of Fig. 3.

As explained by Eq. (3), v_s is driven by the thermal evolutions of the order parameters q , monitoring the spin conversion, and η^2 , monitoring the symmetry change. Figure 5(b) shows the evolution of v_s obtained from Eq. (3) through the thermal evolution of the order parameters, for $(T_{SB} - T_{SC}) = 7$ in the phase diagram. Our model mimics the stepwise lattice contraction measured by neutron diffraction above the triple point, with a discontinuous and hysteretic

change of v_s at the ferroelastic phase transition and a gradual change without hysteresis around the spin crossover. When T_{SB} strongly differs from $T_{1/2}$, the contributions of the nonsymmetry-breaking and symmetry-breaking order parameters to the total volume strain are then clearly separated. This is what Lemée-Cailleau *et al.* [9,43] observed on the lattice parameter of $[\text{Fe}(\text{ptz})_6](\text{BF}_4)_2$ [Fig. 5(a)].

The phase diagram shown in Fig. 2(b) is then in very good agreement with the one of $[\text{Fe}(\text{ptz})_6](\text{BF}_4)_2$ shown in Fig. 2(c) [43], with a first-order phase transition line between HSs ($R\bar{3}$) and LSs ($P\bar{1}$) phases (starting around 140 K, 0 MPa) ending at a triple point around (145 K, 20 MPa). Above the triple point, the transition line splits in two: a first-order ferroelastic transition line from the HSs to the HSls ($P\bar{1}$) and a spin-crossover line from HSls to LSs states. This experimental phase diagram shows that T_{SB} and $T_{1/2}$ evolve differently under pressure and confirms that the $T_{SB} - T_{SC}$ scale in our phase diagram is analogous to pressure.

Miller *et al.* [46] also investigated the evolution of the spin transition of $[\text{Co}(\text{dpzca})_2]$ under pressure. The data illustrate again the different shifts of T_{SB} and $T_{1/2}$ toward higher temperature. The unsymmetric hysteresis loop observed at ambient pressure [Fig. 1(c)] gradually evolves with pressure [Fig. 6(a)] and splits into two distinct processes >0.25 GPa: a partial spin crossover at low temperature and a weaker discontinuous change of the HS fraction γ at high temperature. As pressure increases, the discontinuous changes of γ at high temperature are less and less important. Here again, this apparent stepwise evolution is explained by our model. Figure 6(b) shows the evolution of the order parameters calculated for different $T_{SB} - T_{SC}$, obtained from the potential in Eq. (5). It shows that, when T_{SB} and T_{SC} are close, the spin transition and ferroelastic symmetry breaking occur in a coupled way, resulting in a single and discontinuous spin transition from HSs to LSs, with unsymmetric thermal hysteresis loop. At higher pressure, when $T_{SB} - T_{SC}$ increases, a partial spin crossover occurs first, and a smaller discontinuous change of γ occurs at higher temperature due to the coupling to the ferroelastic distortion. This is also characteristic of the LSls-HSls-HSs sequence of phases, corresponding again to the top panels of Fig. 3.

Even though $[\text{Co}(\text{dpzca})_2]$ and $[\text{Fe}(\text{ptz})_6](\text{BF}_4)_2$ are very different systems, both from the chemistry and crystallography viewpoints, their phase diagrams in terms of spin conversion and ferroelastic phase transition are similar, with a triple point where the HSs, HSls, and LSs phases coexist. Below the triple point, a spin-transition hysteresis loop appears, as both instabilities are coupled. Above the triple point, the spin crossover is separated from the ferroelastic transition, which remains discontinuous for $[\text{Fe}(\text{ptz})_6](\text{BF}_4)_2$ due to the bidimensional nature of η .

There is no such restriction in the case of $[\text{Co}(\text{dpzca})_2]$, and therefore, the ferroelastic phase transition may become continuous at a tricritical point. This may explain the disappearance of the hysteresis at the ferroelastic step in the spin-transition curve of $[\text{Co}(\text{dpzca})_2]$ > 0.29 MPa [Fig. 6(a)]. As explained above, we restricted our model to a constant and negative parameter b for describing a discontinuous ferroelastic transition, as we are interested in the qualitative aspects resulting from the elastic coupling between the

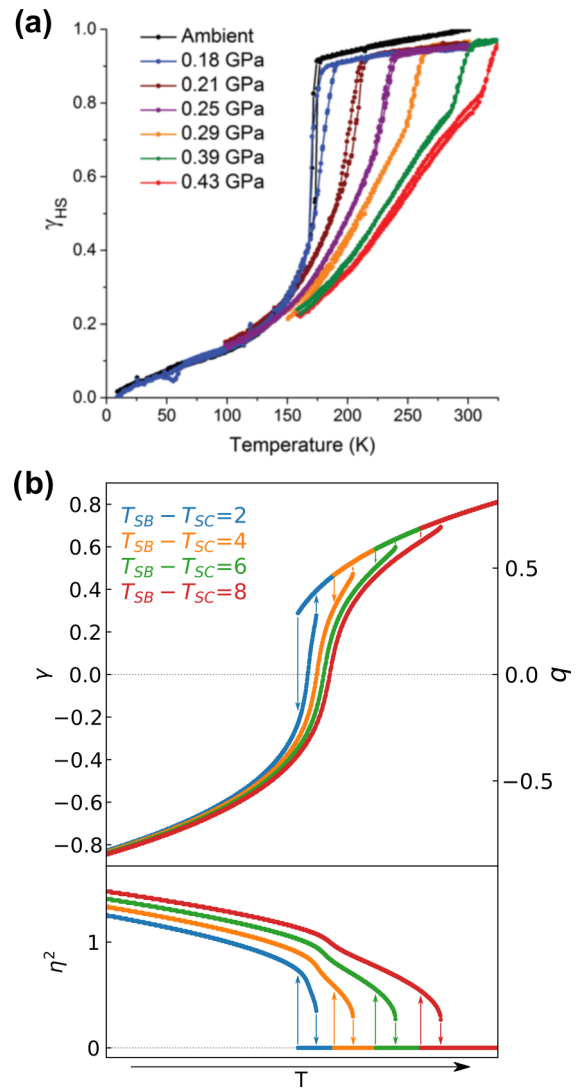


FIG. 6. (a) Evolution from the spin transition at ambient pressure to a spin crossover under pressure for $[\text{Co}(\text{dpzca})_2]$ [46]. (b) Evolution of the order parameters with $T_{SB} - T_{SC}$ obtained from the potential in Eq. (5) for different values of $T_{SB} - T_{SC}$. When $T_{SB} - T_{SC}$ is small, the spin transition and ferroelastic symmetry breaking occur simultaneously, while when $T_{SB} - T_{SC}$ is large, a partial spin crossover occurs first, and a smaller discontinuous change of γ occurs with the ferroelastic distortion.

spin-crossover and the discontinuous ferroelastic transition. Implementing a pressure dependence of the parameters b and B would allow reproducing more qualitatively the experimental observation. However, the space of parameters to explore becomes very large, which is out of the scope of this paper.

In a similar way, the $\text{Fe}(\text{PM-pea})_2(\text{NCS})_2$ and $\text{Fe}(\text{PM-pea})_2(\text{NCSe})_2$ compounds also exhibit spin-transition curves with unsymmetric hysteresis loop [49–51]. However, the phase transitions in these systems are very unusual, as their low-temperature LS phases are hs (LSs orthorhombic), and their HS phases are ls (HSs monoclinic). Here again, the symmetry-breaking order parameter η , driving the orthorhombic-to-monoclinic ferroelastic transition, belongs to the one-dimensional B_{2g} representation of the mmm

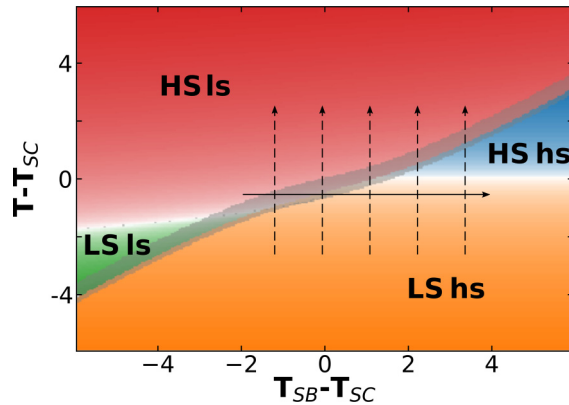


FIG. 7. Phase diagram calculated with the symmetry-adapted 2-4-6 potential in Eq. (5) for $\text{Fe}(\text{PM-pea})_2(\text{NCS})_2$ and $\text{Fe}(\text{PM-pea})_2(\text{NCSe})_2$ using negative values for the coefficients a and D . The horizontal arrow represents the pressure-induced high-spin, low-symmetry (HSIs)–to–low-spin, high-symmetry (LSHs) phase transition. At low pressure, the thermal conversion (left vertical arrow) describes the direct LSHs to HSIs transition. At higher pressure (right vertical arrow), a crossover starts from the LSHs to the HSHs state, followed by a ferroelastic phase transition from HSHs to HSIs. The gray area shows the hysteresis region.

point group [74,75]. The potential in Eq. (5) is symmetry adapted to model this phase transition. For describing the HSIs phase stable at high temperature and the LSHs phase stable at low temperature, the sign of A is changed and $D < 0$, so that the $Dq\eta^2$ coupling term stabilizes the HSIs phase ($q > 0$, $\eta \neq 0$). Figure 7 shows the calculated phase diagram, and Fig. 4(c) shows the spin and symmetry-breaking transition curves calculated just below the triple point. Here again, the spin transition hysteresis loop is unsymmetric due to the $Dq\eta^2$ elastic coupling, distorting the potential in the HSIs phase, where $\eta \neq 0$, compared with the LSHs phase, where $\eta = 0$. X-ray diffraction measurements under pressure, for both $\text{Fe}(\text{PM-pea})_2(\text{NCS})_2$ and $\text{Fe}(\text{PM-pea})_2(\text{NCSe})_2$ [80,81], confirmed that, at room temperature, the HSIs (monoclinic)-to-LSHs (orthorhombic) phase transition occurs under moderate pressure. It corresponds to the horizontal arrow in Fig. 7. Magnetic measurements have shown that the hysteresis loop evolves under pressure: on warming, a partial spin crossover occurs before a discontinuous change of γ , whereas on cooling, the HS fraction change is more discontinuous and shifted to higher temperatures [82], as illustrated by Fig. 7. This situation is therefore similar to the one of $[\text{Co}(\text{dpzca})_2]$ and $[\text{Fe}(\text{ptz})_6](\text{BF}_4)_2$ as it corresponds to a decoupling of the ferroelastic symmetry breaking and the spin crossover. It is also interesting to underline that Taillefer *et al.* [50] reported a second polymorph of $\text{Fe}(\text{PM-pea})_2(\text{NCS})_2$, which undergoes a gradual spin crossover, without symmetry change. This is another illustration that, in this case, the spin-transition hysteresis loop is driven by the symmetry-breaking ferroelastic distortion, as without distortion ($\eta = 0$), the potentials in Eqs. (5) and (7) describe a simple spin crossover.

In the case of the nitroxyl radical Me-AZADO [Fig. 1(b)], and to some extent in the case of the $\text{Fe}(\text{PM-pea})_2(\text{NCS})_2$ and $\text{Fe}(\text{PM-pea})_2(\text{NCSe})_2$ systems, a broadening of the

thermal hysteresis is also observed under pressure. This effect is slightly seen in Fig. 7 and is stronger when a discontinuous ferroelastic phase transition couples to a cooperative spin transition, as discussed in the case of MnFe Prussian blue analogues [26]. Here again, considering the pressure dependence of the coefficient B in the model would allow a more diverse mapping of the different scenarios from spin crossover ($B > 0$) to spin transition ($B < 0$).

III. CONCLUSIONS

Our Landau model, including the most important symmetry-allowed features in the potential, highlights that the elastic coupling between a first-order and symmetry-breaking ferroelastic transition and a nonsymmetry-breaking electronic instability generates different phases and transition lines. The phenomenological approach presented here provides the necessary formalism for describing and disentangling spin transition and symmetry breaking, as well as the associated volume strain, considering the coupling between two order parameters: q (nonsymmetry breaking), monitoring the evolution of the HS fraction γ , and η the symmetry-breaking ferroelastic distortion. We focused our attention on the different phases, which coexist at the triple point. Below the triple point, the difference in the cooperative nature of the cooling and warming branches in the spin-transition hysteresis is due to the $Dq\eta^2$ coupling, responsible for the unsymmetric loops. The cooperative spin transition is then driven by the symmetry-breaking structural phase transition and not driving. Above the triple point, the spin conversion occurs in the form of a spin crossover followed by a discontinuous jump at the ferroelastic phase transition, which may become continuous above a tricritical point.

This model applies to various types of systems for which a nonsymmetry-breaking electronic instability and a ferroelastic distortion couple both to volume strain, and it is not limited to Fe-based (ferrous or ferric) or Co-based spin-crossover materials. Indeed, there are many other examples of spin-crossover materials in the literature exhibiting exotic and unsymmetric hysteresis loops and for which important structural reorganizations come into play. Floquet *et al.* [27] evidenced that the ferric complex $\text{Li}[\text{Fe}(\text{5BrThsa})_2] \cdot \text{H}_2\text{O}$ undergoes a discontinuous spin transition, with 39 K wide thermal hysteresis, coupled to a first order structural phase transition with an important lattice strain as the β angle changes from 101° to 90° . Weber *et al.* [28] reported a similar unsymmetric and 21 K wide thermal hysteresis loop in the case of a dinuclear system coupled to a large volume strain due to the important variation of the triclinic angles. Zhu *et al.* [29] also reported multi-induced spin-crossover behavior for the $[\text{Fe}^{\text{II}}\text{L}_2][\text{ClO}_4]_2$ compound. The unsymmetric thermal spin hysteresis loop is due to the coupling to an orthorhombic-to-monoclinic ferroelastic transition, leading to two inequivalent Fe^{II} sites and a partial spin conversion, as only one site reaches the LS state. Hydrostatic pressure shifts the spin-transition curves toward higher temperature and modifies the shapes of the thermal hysteresis, as shown in Fig. 6(b). The model is also relevant to describe Mn-based materials undergoing spin crossover coupled to monoclinic-triclinic ferroelastic distortion, which is responsible for giant

magnetolectric coupling [47,48]. It also applies for describing many other types of systems, such as MnFe Prussian blue analogues, undergoing a coupled cubic-tetragonal ferroelastic distortion related to Jahn-Teller distortion and coupled to charge transfer [26] or plastic organic crystals exhibiting magnetic bistability [44]. This model offers therefore a broad field of applications for describing and understanding the coupled or uncoupled electronic and symmetry-breaking instabilities in various types of functional materials.

ACKNOWLEDGMENTS

The authors gratefully acknowledge Agence Nationale de la Recherche for financial support under Grant No. ANR-19-CE30-0004 and No. ANR-19-CE07-0027, the University Rennes 1, and the Fondation Rennes 1 for funding. We thank C. Ecolivet, R. Bertoni, and H. Cailleau for scientific discussions.

-
- [1] M. A. Halcrow, *Spin-Crossover Materials: Properties and Applications* (Wiley, Chichester, UK, 2013).
- [2] J. Zarembowitch, F. Varret, A. Hauser, J.-A. Real, and K. Boukheddaden, Preface and introduction, *C.R. Chim.* **21**, 1056 (2018).
- [3] S. Brooker, Spin crossover with thermal hysteresis: Practicalities and lessons learnt, *Chem. Soc. Rev.* **44**, 2880 (2015).
- [4] A. Bhattacharjee, V. Ksenofontov, K. H. Sugiyarto, H. A. Goodwin, and P. Gütllich, Anomalous spin transition observed in bis(2,6-bis(pyrazol-3-yl)pyridine)iron(II) thiocyanate dihydrate, *Adv. Funct. Mater.* **13**, 877 (2003).
- [5] A. Bellec, J. Lagoute, and V. Repain, Molecular electronics: Scanning tunneling microscopy and single-molecule devices, *C.R. Chim.* **21**, 1287 (2018).
- [6] G. Molnár, S. Rat, L. Salmon, W. Nicolazzi, and A. Bousseksou, Spin crossover nanomaterials: From fundamental concepts to devices, *Adv. Mater.* **30**, 1703862 (2018).
- [7] S. P. Vallone, A. N. Tantillo, A. M. dos Santos, J. J. Molaison, R. Kulmaczewski, A. Chapoy, P. Ahmadi, M. A. Halcrow, and K. G. Sandeman, Giant barocaloric effect at the spin crossover transition of a molecular crystal, *Adv. Mater.* **31**, 1807334 (2019).
- [8] A. B. Gaspar, G. Molnár, A. Rotaru, and H. J. Shepherd, Pressure effect investigations on spin-crossover coordination compounds, *C.R. Chim.* **21**, 1095 (2018).
- [9] M. H. Lemée-Cailleau, C. Ecolivet, B. Ouladdiaf, F. Moussa, J. Jeftic, and J. F. Létard, Intermediate ferroelastic phase of the photo-sensible spin-crossover system $[\text{Fe}(\text{ptz})_6](\text{BF}_4)_2$, *J. Magn. Magn. Mater.* **310**, 1792 (2007).
- [10] L. Piñeiro-López, F.-J. Valverde-Muñoz, E. Trzop, M. C. Muñoz, M. Serebyuk, J. Castells-Gil, I. da Silva, C. Martí-Gastaldo, E. Collet, and J. A. Real, Guest induced reversible on-off switching of elastic frustration in a 3D spin crossover coordination polymer with room temperature hysteretic behaviour, *Chem. Sci.* **12**, 1317 (2021).
- [11] K. A. Zenere, S. G. Duyker, E. Trzop, E. Collet, B. Chan, P. W. Doheny, C. J. Kepert, and S. M. Neville, Increasing spin crossover cooperativity in 2D Hofmann-type materials with guest molecule removal, *Chem. Sci.* **9**, 5623 (2018).
- [12] S. Decurtins, P. Gütllich, C. P. Köhler, H. Spiering, and A. Hauser, Light-induced excited spin state trapping in a transition-metal complex: The hexa-1-propyltetrazole-iron (II) tetrafluoroborate spin-crossover system, *Chem. Phys. Lett.* **105**, 1 (1984).
- [13] A. Hauser, P. Adler, S. Deisenroth, P. Gutlich, C. Hennen, H. Spiering, and A. Vef, Intersystem crossing in Fe(II) coordination-compounds, *Hyperfine Interact.* **90**, 77 (1994).
- [14] R. Bertoni, E. Collet, H. Cailleau, M. L. Boillot, A. Tissot, J. Laisney, C. Enachescu, and M. Lorenc, Temperature dependence of the cooperative out-of-equilibrium elastic switching in a spin-crossover material, *Phys. Chem. Chem. Phys.* **21**, 6606 (2019).
- [15] H. T. Lemke, K. S. Kjær, R. Hartsock, T. Brandt van Driel, M. Chollet, J. M. Glowina, S. Song, D. Zhu, E. Pace, S. F. Matar, M. N. Nielsen, M. Benfatto, K. J. Gaffney, E. Collet, and M. Cammarata, Coherent structural trapping through wave packet dispersion during photoinduced spin state switching, *Nat. Commun.* **8**, 15342 (2017).
- [16] S. Zerdane, L. Wilbraham, M. Cammarata, O. Iasco, E. Rivière, M. L. Boillot, I. Ciofini, and E. Collet, Comparison of structural dynamics and coherence of d-d and MLCT light-induced spin state trapping, *Chem. Sci.* **8**, 4978 (2017).
- [17] M. Cammarata, S. Zerdane, L. Balducci, G. Azzolina, S. Mazerat, C. Exertier, M. Trabuco, M. Levantino, R. Alonso-Mori, J. M. Glowina, S. Song, L. Catala, T. Mallah, S. F. Matar, and E. Collet, Charge transfer driven by ultrafast spin transition in a CoFe Prussian blue analogue, *Nat. Chem.* **13**, 10 (2021).
- [18] M. D. Manrique-Juárez, F. Mathieu, A. Laborde, S. Rat, V. Shalabaeva, P. Demont, O. Thomas, L. Salmon, T. Leichle, L. Nicu, G. Molnár, and A. Bousseksou, Micromachining-compatible, facile fabrication of polymer nanocomposite spin crossover actuators, *Adv. Funct. Mater.* **28**, 1801970 (2018).
- [19] K. Ichiyanagi, J. Hebert, L. Toupet, H. Cailleau, P. Guionneau, J.-F. Létard, and E. Collet, Nature and mechanism of the photoinduced spin transition in $[\text{Fe}(\text{PM-BiA})_2(\text{NCS})_2]$, *Phys. Rev. B* **73**, 060408(R) (2006).
- [20] M. Buron-Le Cointe, J. Hébert, C. Baldé, N. Moisan, L. Toupet, P. Guionneau, J. F. Létard, E. Freysz, H. Cailleau, and E. Collet, Intermolecular control of thermoswitching and photoswitching phenomena in two spin-crossover polymorphs, *Phys. Rev. B* **85**, 064114 (2012).
- [21] K. W. Törnroos, M. Hostettler, D. Chernyshov, B. Vangdal, and H.-B. Bürgi, Interplay of spin conversion and structural phase transformations: Re-entrant phase transitions in the 2-propanol solvate of tris(2-picolylamine)iron(II) dichloride, *Chemistry—A European Journal* **12**, 6207 (2006).
- [22] S. Lakhloufi, P. Guionneau, M. H. Lemée-Cailleau, P. Rosa, and J. F. Létard, Structural phase transition in the spin-crossover complex $[\text{Fe}(\text{ptz})_6](\text{BF}_4)_2$ studied by x-ray diffraction, *Phys. Rev. B* **82**, 132104 (2010).
- [23] V. A. Money, J. Elhaik, I. Radosavljevic Evans, M. A. Halcrow, and J. A. K. Howard, A study of the thermal and light induced spin transition in $[\text{FeL}_2](\text{BF}_4)_2$ and $[\text{FeL}_2](\text{ClO}_4)_2$

- $L = 2$, 6-di(3-methylpyrazol-1-yl)pyrazine, *Dalton Trans.*, **65** (2004).
- [24] G. A. Craig, J. Sánchez-Costa, O. Roubeau, S. J. Teat, and G. Aromí, Coupled crystallographic order–disorder and spin state in a bistable molecule: Multiple transition dynamics, *Chemistry—A European Journal* **17**, 3120 (2011).
- [25] A. Djemel, O. Stefanczyk, M. Marchivie, E. Trzop, E. Collet, C. Desplanches, R. Delimi, and G. Chastanet, Solvatomorphism-induced 45 K hysteresis width in a spin-crossover mononuclear compound, *Chemistry—A European Journal* **24**, 14760 (2018).
- [26] G. Azzolina, R. Bertoni, C. Ecolivet, H. Tokoro, S.-i. Ohkoshi, and E. Collet, Landau theory for non-symmetry-breaking electronic instability coupled to symmetry-breaking order parameter applied to Prussian blue analog, *Phys. Rev. B* **102**, 134104 (2020).
- [27] S. Floquet, N. Guillou, P. Négrier, E. Rivière, and M.-L. Boillot, The crystallographic phase transition for a ferric thiosemicarbazone spin crossover complex studied by x-ray powder diffraction, *New J. Chem.* **30**, 1621 (2006).
- [28] B. Weber, E. S. Kaps, J. Obel, K. Achterhold, and F. G. Parak, Synthesis and characterization of a dinuclear iron(II) spin crossover complex with wide hysteresis, *Inorg. Chem.* **47**, 10779 (2008).
- [29] Y.-Y. Zhu, C.-W. Liu, J. Yin, Z.-S. Meng, Q. Yang, J. Wang, T. Liu, and S. Gao, Structural phase transition in a multi-induced mononuclear FeII spin-crossover complex, *Dalton Trans.* **44**, 20906 (2015).
- [30] E. K. Salje, *Phase Transitions in Ferroelastic and Co-Elastic Crystals* (Cambridge Topics in Mineral Physics and Chemistry), (Cambridge University Press, Cambridge, 1991).
- [31] B. Weber, W. Bauer, and J. Obel, An iron(II) spin-crossover complex with a 70 K wide thermal hysteresis loop, *Angew. Chem. Int. Ed.* **47**, 10098 (2008).
- [32] M. Seredyuk, M. C. Muñoz, M. Castro, T. Romero-Morcillo, A. B. Gaspar, and J. A. Real, Unprecedented multi-stable spin crossover molecular material with two thermal memory channels, *Chemistry—A European Journal* **19**, 6591 (2013).
- [33] M. A. Halcrow, Spin-crossover compounds with wide thermal hysteresis, *Chem. Lett.* **43**, 1178 (2014).
- [34] M. G. Reeves, E. Tailleu, P. A. Wood, M. Marchivie, G. Chastanet, P. Guionneau, and S. Parsons, Mapping the cooperativity pathways in spin crossover complexes, *Chem. Sci.* **12**, 1007 (2021).
- [35] E. Collet and P. Guionneau, Structural analysis of spin-crossover materials: From molecules to materials, *C.R. Chim.* **21**, 1133 (2018).
- [36] P. Gutlich, Y. Garcia, and H. A. Goodwin, Spin crossover phenomena in Fe(II) complexes, *Chem. Soc. Rev.* **29**, 419 (2000).
- [37] J. Kusz, M. Zubko, R. B. Neder, and P. Gutlich, Structural phase transition to disorder low-temperature phase in $[\text{Fe}(\text{ptz})_6](\text{BF}_4)_2$ spin-crossover compounds, *Acta Cryst.* **68**, 40 (2012).
- [38] A. Marino, P. Chakraborty, M. Servol, M. Lorenc, E. Collet, and A. Hauser, The role of ligand-field states in the ultrafast photophysical cycle of the prototypical iron(II) spin-crossover compound $[\text{Fe}(\text{ptz})_6](\text{BF}_4)_2$, *Angew. Chem. Int. Ed.* **53**, 3863 (2014).
- [39] C. Chong, H. Mishra, K. Boukheddaden, S. Denise, G. Bouchez, E. Collet, J. C. Ameline, A. D. Naik, Y. Garcia, and F. Varret, Electronic and structural aspects of spin transitions observed by optical microscopy. The case of $[\text{Fe}(\text{ptz})_6](\text{BF}_4)_2$, *J. Phys. Chem. B* **114**, 1975 (2010).
- [40] A. Goujon, F. Varret, K. Boukheddaden, C. Chong, J. Jeftić, Y. Garcia, A. D. Naik, J. C. Ameline, and E. Collet, An optical microscope study of photo-switching and relaxation in single crystals of the spin transition solid $[\text{Fe}(\text{ptz})_6](\text{BF}_4)_2$, with image processing, *Inorg. Chim. Acta* **361**, 4055 (2008).
- [41] A. Hauser, Cooperative effects on the Hs \rightarrow Ls relaxation in the $[\text{Fe}(\text{ptz})_6](\text{BF}_4)_2$ spin-crossover system, *Chem. Phys. Lett.* **192**, 65 (1992).
- [42] A. Hauser, Intersystem crossing in the $[\text{Fe}(\text{ptz})_6](\text{BF}_4)_2$ spin crossover system (ptz = 1-propyltetrazole), *J. Chem. Phys.* **94**, 2741 (1991).
- [43] M.-H. Lemée-Cailleau, C. Ecolivet, B. Ouladdiaf, F. Moussa, and J.-F. Létard, Multi-phase spin crossover in $[\text{Fe}(\text{ptz})_6](\text{BF}_4)_2$, *Physica B* **404**, 379 (2009).
- [44] A. Dragulescu-Andrasi, A. S. Filatov, R. T. Oakley, X. Li, K. Lekin, A. Huq, C. Pak, S. M. Greer, J. McKay, M. Jo, J. Lengyel, I. Hung, E. Maradzike, A. E. DePrince, III, S. A. Stoian, S. Hill, Y. Y. Hu, and M. Shatruk, Radical dimerization in a plastic organic crystal leads to structural and magnetic bistability with wide thermal hysteresis, *J. Am. Chem. Soc.* **141**, 17989 (2019).
- [45] M. G. Cowan, J. Olguín, S. Narayanaswamy, J. L. Tallon, and S. Brooker, Reversible switching of a cobalt complex by thermal, pressure, and electrochemical stimuli: Abrupt, complete, hysteretic spin crossover, *J. Am. Chem. Soc.* **134**, 2892 (2012).
- [46] R. G. Miller, S. Narayanaswamy, S. M. Clark, P. Dera, G. B. Jameson, J. L. Tallon, and S. Brooker, Pressure induced separation of phase-transition-triggered-abrupt vs. gradual components of spin crossover, *Dalton Trans.* **44**, 20843 (2015).
- [47] V. B. Jakobsen, E. Trzop, L. C. Gavin, E. Dobbelaar, S. Chikara, X. Ding, K. Esien, H. Müller-Bunz, S. Felton, V. S. Zapf, E. Collet, M. A. Carpenter, and G. G. Morgan, Stress-induced domain wall motion in a ferroelastic Mn^{3+} spin crossover complex, *Angew. Chem. Int. Ed.* **59**, 13305 (2020).
- [48] V. B. Jakobsen, S. Chikara, J.-X. Yu, E. Dobbelaar, C. T. Kelly, X. Ding, F. Weickert, E. Trzop, E. Collet, H.-P. Cheng, G. G. Morgan, and V. S. Zapf, Giant magnetoelectric coupling and magnetic-field-induced permanent switching in a spin crossover Mn(III) complex, *Inorg. Chem.* (2020), doi: 10.1021/acs.inorgchem.0c02789.
- [49] P. Guionneau, J. F. Letard, D. S. Yufit, D. Chasseau, G. Bravic, A. E. Goeta, J. A. K. Howard, and O. Kahn, Structural approach of the features of the spin crossover transition in iron(II) compounds, *J. Mater. Chem.* **9**, 985 (1999).
- [50] E. Tailleu, M. Marchivie, P. Négrier, D. Denux, S. Massip, D. Mondieig, G. Chastanet, and P. Guionneau, Using polymorphism to master the spin crossover mechanism in $[\text{Fe}(\text{PM-PeA})_2(\text{NCSe})_2]$, *CrystEngComm* **21**, 6246 (2019).
- [51] J.-F. Létard, P. Guionneau, E. Codjovi, O. Lavastre, G. Bravic, D. Chasseau, and O. Kahn, Wide thermal hysteresis for the mononuclear spin-crossover compound cis-bis(thiocyanato) bis[N-(2'-pyridylmethylene)-4-(phenylethynyl)anilino]iron(II), *J. Am. Chem. Soc.* **119**, 10861 (1997).
- [52] W. Nicolazzi and A. Bousseksou, Thermodynamical aspects of the spin crossover phenomenon, *C.R. Chim.* **21**, 1060 (2018).

- [53] M. Paez-Espejo, M. Sy, and K. Boukheddaden, Elastic frustration causing two-step and multistep transitions in spin-crossover solids: Emergence of complex antiferroelastic structures, *J. Am. Chem. Soc.* **138**, 3202 (2016).
- [54] H. Spiering and N. Willenbacher, Elastic interaction of high-spin and low-spin complex molecules in spin-crossover compounds. II, *J. Phys. Condens. Matter* **1**, 10089 (1989).
- [55] C. Enachescu, L. Stoleriu, M. Nishino, S. Miyashita, A. Stancu, M. Lorenc, R. Bertoni, H. Cailleau, and E. Collet, Theoretical approach for elastically driven cooperative switching of spin-crossover compounds impacted by an ultrashort laser pulse, *Phys. Rev. B* **95**, 224107 (2017).
- [56] A. Bousseksou, G. Molnar, L. Salmon, and W. Nicolazzi, Molecular spin crossover phenomenon: Recent achievements and prospects, *Chem. Soc. Rev.* **40**, 3313 (2011).
- [57] P. Gutlich, A. Hauser, and H. Spiering, Thermal and optical switching of iron(II) complexes, *Angew. Chem. Int. Ed.* **33**, 2024 (1994).
- [58] A. Bousseksou, J. J. McGarvey, F. Varret, J. A. Real, J.-P. Tuchagues, A. C. Dennis, and M. L. Boillot, Raman spectroscopy of the high- and low-spin states of the spin crossover complex $\text{Fe}(\text{phen})_2(\text{NCS})_2$: An initial approach to estimation of vibrational contributions to the associated entropy change, *Chem. Phys. Lett.* **318**, 409 (2000).
- [59] H. Spiering, K. Boukheddaden, J. Linares, and F. Varret, Total free energy of a spin-crossover molecular system, *Phys. Rev. B* **70**, 184106 (2004).
- [60] J. Pavlik and J. Linares, Microscopic models of spin crossover, *C.R. Chim.* **21**, 1170 (2018).
- [61] L. Stoleriu, P. Chakraborty, A. Hauser, A. Stancu, and C. Enachescu, Thermal hysteresis in spin-crossover compounds studied within the mechanoelastic model and its potential application to nanoparticles, *Phys. Rev. B* **84**, 134102 (2011).
- [62] C. P. Slichter and H. G. Drickamer, Pressure-induced electronic changes in compounds of iron, *J. Chem. Phys.* **56**, 2142 (1972).
- [63] J. Cruddas and B. J. Powell, Structure-property relationships and the mechanisms of multistep transitions in spin crossover materials and frameworks, *Inorg. Chem. Front.* **7**, 4424 (2020).
- [64] A. Slimani, K. Boukheddaden, and K. Yamashita, Effect of intermolecular interactions on the nucleation, growth, and propagation of like-spin domains in spin-crossover materials, *Phys. Rev. B* **92**, 014111 (2015).
- [65] C. Enachescu and W. Nicolazzi, Elastic models, lattice dynamics and finite size effects in molecular spin crossover systems, *C.R. Chim.* **21**, 1179 (2018).
- [66] H. Watanabe, K. Tanaka, N. Bréfuel, H. Cailleau, J.-F. Létard, S. Ravy, P. Fertey, M. Nishino, S. Miyashita, and E. Collet, Ordering phenomena of high-spin/low-spin states in stepwise spin-crossover materials described by the ANNNI model, *Phys. Rev. B* **93**, 014419 (2016).
- [67] A. Marino, M. Buron-Le Cointe, M. Lorenc, L. Toupet, R. Henning, A. D. DiChiara, K. Moffat, N. Bréfuel, and E. Collet, Out-of-equilibrium dynamics of photoexcited spin-state concentration waves, *Faraday Discuss.* **177**, 363 (2015).
- [68] R. Traiche, M. Sy, and K. Boukheddaden, Elastic frustration in 1D spin-crossover chains: Evidence of multi-step transitions and self-organizations of the spin states, *J. Phys. Chem. C* **122**, 4083 (2018).
- [69] D. Chernyshov, N. Klinduhov, K. W. Törnroos, M. Hostettler, B. Vangdal, and H.-B. Bürgi, Coupling between spin conversion and solvent disorder in spin crossover solids, *Phys. Rev. B* **76**, 014406 (2007).
- [70] M. A. Carpenter, E. K. H. Salje, and A. Graeme-Barber, Spontaneous strain as a determinant of thermodynamic properties for phase transitions in minerals, *Eur. J. Mineral.* **10**, 621 (1998).
- [71] C. Enachescu, M. Nishino, S. Miyashita, K. Boukheddaden, F. Varret, and P. A. Rikvold, Shape effects on the cluster spreading process of spin-crossover compounds analyzed within an elastic model with Eden and Kawasaki dynamics, *Phys. Rev. B* **91**, 104102 (2015).
- [72] K. Boukheddaden, I. Shteto, B. Hôo, and F. Varret, Dynamical model for spin-crossover solids. II. Static and dynamic effects of light in the mean-field approach, *Phys. Rev. B* **62**, 14806 (2000).
- [73] G. Azzolina, R. Bertoni, and E. Collet, General Landau theory of non-symmetry-breaking and symmetry-breaking spin transition materials, *J. Appl. Phys.* **129**, 085106 (2021).
- [74] V. Janovec and J. Privratska, Domain structures, in *International Tables for Crystallography* (Wiley & Sons Ltd, West Sussex, 2006), Vol. D, Chap. 3.4, p. 449.
- [75] V. Janovec, V. Dvořák, and J. Petzelt, Symmetry classification and properties of equi-translation structural phase transitions, *Czech. J. Phys.* **25**, 1362 (1975).
- [76] L. Wiehl, Structures of hexakis(1-propyltetrazole)iron(II) bis(tetrafluoroborate), $[\text{Fe}(\text{CHN}_4\text{C}_3\text{H}_7)_6](\text{BF}_4)_2$, hexakis(1-methyltetrazole)iron(II) bis(tetrafluoroborate), $[\text{Fe}(\text{CHN}_4\text{CH}_3)_6](\text{BF}_4)_2$, and the analogous perchlorates. Their relation to spin crossover behaviour and comparison of Debye-Waller factors from structure determination and Mossbauer spectroscopy, *Acta Cryst.* **B49**, 289 (1993).
- [77] L. Wiehl, H. Spiering, P. Gutlich, and K. Knorr, Calculation of the lattice deformation at the phase transitions of $[\text{Fe}(\text{ptz})_6](\text{BF}_4)_2$ from powder diffraction patterns, *J. Appl. Crystallogr.* **23**, 151 (1990).
- [78] J. D. Axe and Y. Yamada, Cubic-tetragonal elastic phase transformations in solids, *Phys. Rev. B* **24**, 2567 (1981).
- [79] P. Toledano, M. M. Fejer, and B. A. Auld, Nonlinear elasticity in proper ferroelastics, *Phys. Rev. B* **27**, 5717 (1983).
- [80] N. Paradis, F. Le Gac, P. Guionneau, A. Largeau, D. Yufit, P. Rosa, J.-F. Létard, and G. Chastanet, Effects of internal and external pressure on the $[\text{Fe}(\text{PM-PEA})_2(\text{NCS})_2]$ spin-crossover compound (with $\text{PM-PEA} = \text{N}-(2'$ -pyridylmethylene)-4-(phenylethynyl)aniline), *Magnetochemistry* **2**, 15 (2016).
- [81] E. Tailleur, M. Marchivie, J. P. Itie, P. Rosa, N. Daro, and P. Guionneau, Pressure-induced spin-crossover features at variable temperature revealed by in situ synchrotron powder x-ray diffraction, *Chemistry* **24**, 14495 (2018).
- [82] V. Ksenofontov, G. Levchenko, H. Spiering, P. Gutlich, J. F. Létard, Y. Bouhedja, and O. Kahn, Spin crossover behavior under pressure of $\text{Fe}(\text{PM-L})_2(\text{NCS})_2$ compounds with substituted 2'-pyridylmethylene 4-anilino ligands, *Chem. Phys. Lett.* **294**, 545 (1998).